International Research Journal of Advanced Engineering and Science
ISSN (Online): 2455-9024

Machine Learning-Based Prediction of Clad Geometry in Direct Laser Metal Deposition of Inconel 718

Van Toan Nguyen, Duong Van Nguy
Faculty of Mechanical Engineering, Le Quy Don Technical University, Viet Nam
*E-mail: nguyentoan@mta.edu.vn

Abstract— *A critical challenge in Direct Laser Metal Deposition (DLMD) is the precise control of clad geometry to satisfy stringent part specifications. This study presents an integrated experimental and machine learning (ML) framework to predict and optimize the geometrical characteristics of Inconel 718 clads deposited on SS 316L substrates. The relationships between key process parameters, including laser power, scanning speed, and powder feed rate, and the resulting clad geometry (width, height, and depth) were systematically investigated using experimental data. The experimental results reveal that increasing laser power or decreasing scanning speed significantly enlarges clad dimensions, highlighting the dominant role of energy input in governing clad morphology. To capture these complex nonlinear relationships, a Backpropagation Neural Network (BPNN) model was developed, demonstrating high predictive accuracy with coefficients of determination (R^2) of 0.965, 0.952, and 0.961 for clad width, height, and depth, respectively. Furthermore, a hybrid optimization approach combining the trained ML model with Non-dominated Sorting Genetic Algorithm II (NSGA-II) to systematically identify optimal process parameter combinations for improved clad quality. The proposed framework enables efficient multi-objective optimization while reducing the need for extensive experimental trials*.

Keywords— *DLMD, Inconel 718, Machine learning, Process parameters*.

I. INTRODUCTION

Direct laser metal deposition (DLMD) is an advanced additive manufacturing technique that enables the fabrication and repair of metallic components through the localized melting of metal powder by a high-energy laser source [1–3]. One of the key challenges in DLMD is controlling the geometry of the deposited metal trace to meet specific part specifications [4,5]. The geometry of the deposited layer, including width, height, and contour, significantly influences the mechanical properties, surface finish, and overall performance of the final part [4,6,7]. As such, the precise control of the deposition process is crucial, particularly when working with high-performance alloys such as Inconel 718, a nickel-based superalloy widely used in aerospace, power generation, and other high-temperature applications.

In DLMD, the process parameters such as laser power, scanning speed, and powder feed rate have a direct impact on the deposited geometry. The interaction between these parameters determines the thermal behavior, solidification dynamics, and microstructure of the deposited metal. However, achieving the desired clad geometry often requires extensive experimentation due to the complex, nonlinear relationships between process variables and the final product. This complexity increases when dealing with high-performance materials like Inconel 718, which possess unique thermal and mechanical properties that influence the deposition process. Furthermore, the optimization of DLMD processes remains a significant challenge due to the interactions among multiple parameters, expansive solution spaces, and intricate physical metallurgical phenomena. These complexities make conventional trial-and-error methods and numerical simulations both computationally intensive and economically impractical.

To address these challenges, this study proposes a ML based approach to predict the geometrical characteristics of Inconel 718 clads in DLMD [8–10]. ML provides a powerful alternative by leveraging extensive process data to expedite experimental iterations, alleviate computational demands, and facilitate accurate prediction and optimization of process parameters. For example, Liu et al. [6] adopted a hybrid modeling strategy that integrates a Genetic Algorithm with artificial neural networks to predict the geometric characteristics of single track clads fabricated using a high power diode laser. Lim et al. [11] implemented multiple ML algorithms, including Random Forest, Support Vector Machine (SVM), to select manufacturing conditions for a titanium alloy powder DED process. Zhang et al. [12] developed a differential evolution–optimized multi-output support vector regression (DE-MOSVR) model to accurately predict bead morphology in aluminum wire laser hybrid directed energy deposition processes.

This study integrates ML with multi-objective optimization to develop a predictive framework for the clad geometry of Inconel 718 alloy fabricated via DLMD. A full-factorial experimental framework based on the Central Composite Design (CCD) was adopted, with laser power (P), powder feed rate (F), and scan speed (V) defined as input parameters, and height (H), depth (D), and bead width (W) selected as response metrics. Clad geometry prediction was carried out using three different ML algorithms. Subsequently, a multi-objective optimization approach based on the Non-dominated Sorting Genetic Algorithm II (NSGA-II) was utilized to identify Pareto optimal process parameter combinations, with the objective of enhancing bead width and height while reducing penetration depth. Finally, the predicted optimal parameters were experimentally validated.

Van Toan Nguyen and Duong Van Nguy "Machine Learning-Based Prediction of Clad Geometry in Direct Laser Metal Deposition of Inconel 718," *International Research Journal of Advanced Engineering and Science*, Volume 11, Issue 2, pp. 66-71, 2026.

International Research Journal of Advanced Engineering and Science
ISSN (Online): 2455-9024

II. EXPERIMENTAL AND METHODS

2.1. Description of the experimental setup

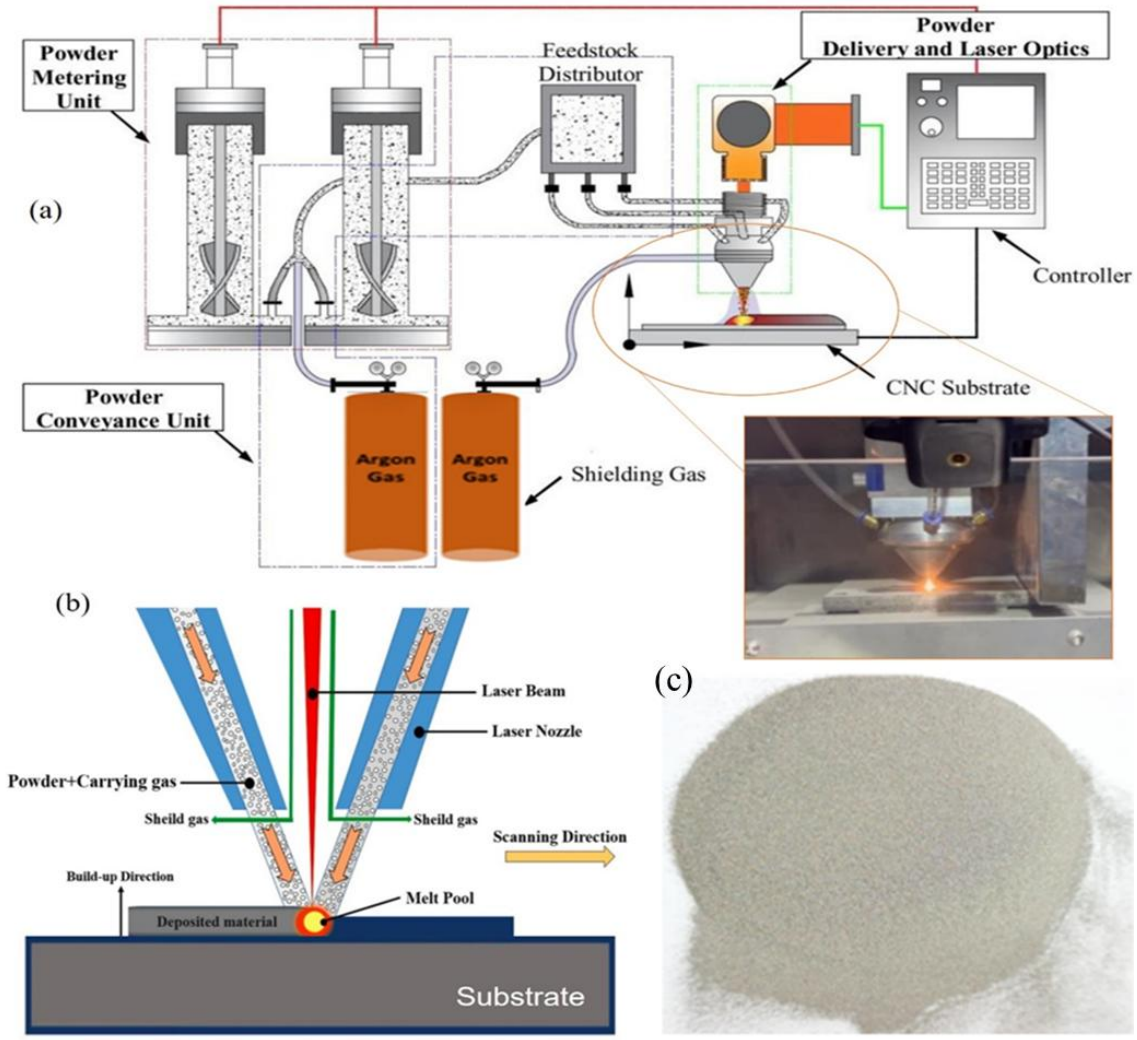

Figure 1. (a) Schematic of the experimental setup, (b) The fabrication principles of the DLMD process, and (c) Iconel 718 powder in this work

Figure 1a provides a schematic representation of the Direct Laser Metal Deposition (DLMD) process. The DLMD experiments were performed using a coaxial powder-fed laser deposition system. The system consists of a three-axis CNC motion platform, a coaxial powder-delivery nozzle, a shielding-gas supply unit, and a high-power fiber laser. A fiber laser operating in continuous-wave mode was employed, featuring a minimum focal spot size of 0,2 mm, a Rayleigh length of 2.0 mm, a focal length of 200 mm, and a wavelength of 1080 nm. Fig. 1b illustrates the operational principles and sequential stages of the process, and Fig. 1c shows the Inconel 718 powder used in this study. The powder was delivered using a metered powder feeder equipped with a rotating-disk mechanism to maintain a stable and controllable mass flow rate. It was transported by high-purity argon and injected coaxially into the melt pool through a multi-jet deposition nozzle. A flat SS316L steel substrate (200×100×10 mm) was horizontally mounted on the build platform, mechanically cleaned, and degreased prior to processing to ensure proper adhesion. During deposition, an argon shielding-gas stream was directed around the melt pool to minimize oxidation and prevent contamination. The entire DLMD system was operated through an integrated CNC controller that regulated the laser power, scanning speed, powder feed rate, and gas flow rate according to the predefined processing parameters.

Figure 2a illustrates the characteristic geometrical parameters extracted from the cross-section of the deposited track. FE-SEM images were analyzed using ImageJ software to determine the geometric characteristics of the deposited layer, including width (W) and height (h). For cross-sectional evaluation, samples produced under each processing condition were sectioned and mechanically prepared. After being polished to a mirror finish, the specimens were chemically etched at room temperature using an aqueous solution of 10% hydrofluoric acid and 15% nitric acid. The cross-sectional morphology of a deposited metal trace fabricated under selected

International Research Journal of Advanced Engineering and Science
ISSN (Online): 2455-9024

DLMD parameters (500 W laser power, 3 mm/s scanning speed, and 100 mg/s powder feed rate) is shown in Fig. 2b.

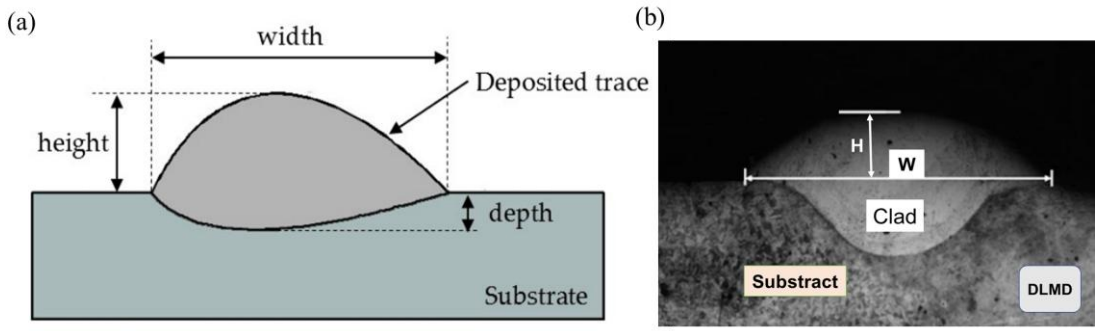

Figure 2. (a) Geometrical parameters of single tracks fabricated by DLMD, and (b) Cross-sectional macrostructure of the deposited metal track.

TABLE 1. Chemical composition of the Inconel 718 powder [13]

Chemical composition										
Element	**Ni**	**Cr**	**Fe**	**Nb**	**Mo**	**Al**	**Si**	**Mn**	**Ti**	**Co**
Wt (%)	53,6	18,2	Bal	5,06	3,04	0,44	0,1	0.163	0,97	0.07

Elemental analysis of the Inconel 718 powder was performed using an ICP system (ES-730; SpectroArcos–AMETEK). The chemical composition obtained from the ICP measurements is summarized in Table 1.

As depicted in Fig. 3, the morphology of Inconel 718 powder particles was investigated using FESEM (MIRA3, TESCAN, Czech Republic). The SEM analysis provides detailed information on particle shape, surface texture, and sphericity, which are key factors affecting powder flowability and packing behavior. These properties play a crucial role in determining process stability, melt pool dynamics, and the resulting microstructural quality of DLMD-fabricated components. For DLMD sample preparation, the substrate surfaces were mechanically ground to achieve a smooth finish with a surface roughness of approximately 0.8 μm. Prior to deposition, surface contaminants such as grease and residues were removed with acetone, and the native oxide layer was eliminated using a stainless-steel brush to ensure proper adhesion and consistent deposition quality.

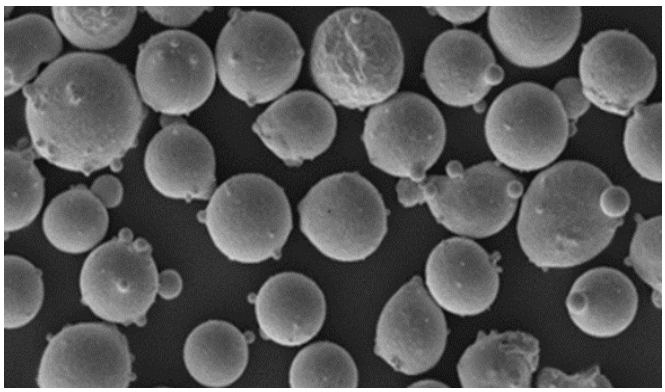

Figure 3. The image of SEM of used IN 718 powder

Key process parameters include laser power, which controls the rate of material heating; scanning speed, which affects melt pool dimensions; and powder feed rate, which plays a critical role in melting efficiency and the resulting microstructure, thereby influencing layer uniformity, thermal gradients, and overall build quality. A broad range of process parameters was defined to generate the training dataset for the ML models, as detailed in Table 2.

TABLE 2. Experimental factors and their corresponding levels

Independent variables	**Units**	**Factor Level**		
		Level 1(-1)	**Level 2(0)**	**Level 3(+1)**
Laser power (P)	W	300	400	500
Scan speed (V)	mm/s	3	5	7
Powder feeding rate (F)	mg/s	100	200	300

2.2. Machine Learning Model Development

In this study, widely adopted ML models, including Support Vector Regression (SVR) and Backpropagation Neural Networks (BPNN), were utilized to predict the geometric characteristics of the deposited layer. Prior to training, all features were normalized to the range of 0–1 using the MinMaxScaler method. This preprocessing step reduces sensitivity to noise, ensures consistent feature scaling, facilitates faster convergence, alleviates gradient-related issues, and enhances overall model generalization.

The dataset was randomly partitioned into training (70%) and testing (30%) subsets using the train–test split function in the Scikit-learn model_selection module (Python 3.9.7). Data processing and model development were performed in Python using key libraries, including NumPy, Pandas, Scikit-learn, XGBoost, and TensorFlow. Hyperparameter tuning was conducted via grid search combined with five-fold cross-validation to mitigate overfitting. The optimal configuration was subsequently used to build the final models, which were then serialized using the pickle module for subsequent multi-objective optimization.

Model performance was evaluated using these metrics, as expressed in the equations below.

International Research Journal of Advanced Engineering and Science
ISSN (Online): 2455-9024

$$RMSE = \sqrt{\frac{1}{n}\sum_{i=1}^{n}(y_i - \hat{y}_i)^2} \quad (1)$$

$$R^2 = 1 - \sum_{i=1}^{n}(y_i - \hat{y}_i)^2 / \sum_{i=1}^{n}(y_i - \bar{y}_i)^2 \quad (2)$$

here y_i denotes the actual value, $\hat{y}_i$ represents the predicted value, $\bar{y}_i$ is the mean value, and n represents the total number of samples.

The Root Mean Squared Error (RMSE) was used to evaluate prediction accuracy, whereas the coefficient of determination (R^2) was employed to assess model fit, with lower RMSE and higher R^2 values indicating better performance.

III. Results and Discussion

A. Influence of Process Parameters on Clad Geometry

Figure 4 illustrates a cross-sectional morphology of the metal track deposited under varying processing parameters. The results indicate that, at fixed scan speed and powder feed rate, increasing laser power leads to a systematic enlargement of the clad geometry, as reflected by greater width, height, and cross-sectional area. Conversely, when laser power and powder feed rate are maintained constant, decreasing the scan speed promotes a noticeable increase in bead dimensions, including width, height, and penetration depth, highlighting the critical role of energy input in governing clad morphology. These observations highlight notable changes in the shape and characteristics of the deposit. The variations in track height, width, and penetration into the substrate are directly linked to the input energy and the heat transfer conditions during deposition. Under specific processing conditions, the deposited track demonstrates relatively symmetrical profiles with distinct boundary interfaces, indicating stable melting and solidification that foster strong metallurgical bonding. In contrast, alternative parameter settings lead to uneven track profiles or inconsistent substrate penetration, suggesting a mismatch between the deposition rate and energy input, which can compromise both the geometric integrity and structural cohesion of the deposited layer.

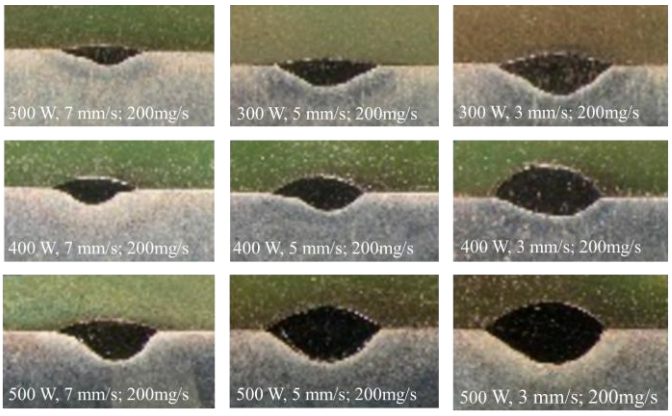

Figure 4. Cross-sectional features of deposited metal tracks obtained under different processing parameters.

The melting behavior of both the substrate and the injected powder is primarily dictated by the interplay between laser power and scan speed, which consequently governs the resulting clad geometry and material characteristics. Inadequate laser power tends to promote lack of fusion and porosity, whereas excessive power intensifies heat accumulation, potentially inducing thermal stresses, geometric distortion, and the formation of residual stresses within the deposited layer [14]. Similarly, excessively low scan speeds promote pronounced dilution due to increased energy input per unit length, whereas overly high scan speeds limit melt pool formation, leading to incomplete fusion and the emergence of porosity [15]. Moreover, the cladding morphology is strongly influenced by both the attenuation of the laser beam caused by the injected metal powders and the convective heat transfer induced by the carrier gas flow over the melt pool. Consequently, predicting the coating morphology solely based on cross-sectional images of the deposited cladding is challenging.

B. Machine learning-based predictive capability

The DLMD process parameters are closely related to the cladding geometry during deposition. Therefore, establishing a direct correlation between input parameters and deposition layer formation is essential.

Figure 5 illustrates that the two ML models differ significantly in their ability to predict cladding width. As shown in the figure, the data points in both datasets are distributed close to the diagonal, indicating that the models exhibit generally good predictive capability for cladding width. However, a few points display relatively large deviations between the predicted and actual values.

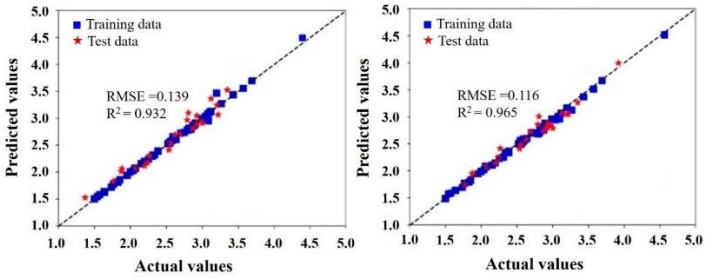

Figure 5. Comparison of prediction accuracy between ML models for cladding width. (a) SVR; (b) BPNN.

These discrepancies may stem from the models' limited ability to capture local outliers within the overall trend or from imbalanced sample distribution in the dataset. The SVR model (Fig. 5a) exhibits larger scatter and occasional discrepancies. In contrast, the BPNN model (Fig. 5b) demonstrates a relatively stable prediction trend with smaller deviations between predicted and experimental values, indicating strong generalization ability and robustness to data variability, suggesting a higher sensitivity to training data and potential overfitting. Overall, the comparative results indicate that BPNN provides more reliable and consistent predictions for cladding width, highlighting its suitability for modeling complex nonlinear relationships in the cladding process.

Fig. 6 illustrates that both ML models can predict cladding height with reasonable accuracy, as evidenced by the general alignment of the predicted values with the diagonal reference line. Nevertheless, clear differences in predictive performance are evident. The SVR model (Fig. 6a) exhibits a broader

Van Toan Nguyen and Duong Van Nguy "Machine Learning-Based Prediction of Clad Geometry in Direct Laser Metal Deposition of Inconel 718," *International Research Journal of Advanced Engineering and Science*, Volume 11, Issue 2, pp. 66-71, 2026.

International Research Journal of Advanced Engineering and Science
ISSN (Online): 2455-9024

dispersion of data points and larger prediction errors in specific regions, resulting in R^2 value of 0.912 and RMSE of 0.089 mm. In contrast, the BPNN model (Fig. 6b) shows a tighter clustering of predicted values along the ideal fitting line, achieving a higher R^2 of 0.952 and a lower RMSE of 0.071 mm.

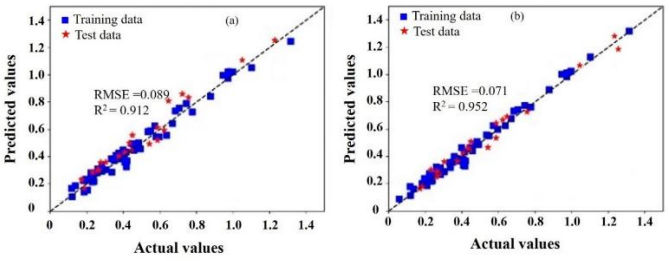

Figure 6. Comparison of prediction accuracy between ML models for cladding height: (a) SVR; (b) BPNN.

This improvement suggests that the BPNN model is more effective in capturing the nonlinear relationship between process parameters and cladding height. Overall, the selected input variables account for approximately 95.2% and 91.2% of the variance in cladding height for the BPNN and SVR models, respectively, confirming the superior predictive performance of the BPNN model in capturing the complex relationship between process parameters and cladding height.

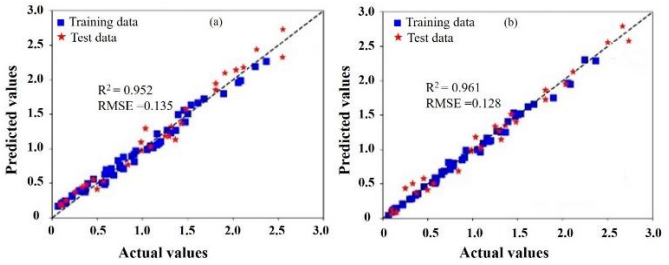

Figure 7. Comparative evaluation of prediction accuracy for cladding depth using ML models: (a) SVR; (b) BPNN.

Figure 7 presents a comparison of the predictive performance of the SVR and BPNN models in estimating cladding depth. Both models show good agreement between the predicted and experimental values, confirming their capability to model the cladding depth response, with R^2 values exceeding 0.95. However, distinct differences in prediction accuracy are observed. The SVR model (Fig. 7a) presents a more scattered distribution of data points with noticeable deviations in certain regions, indicating limitations in capturing complex nonlinear relationships (R^2 = 0.952, RMSE = 0.135 mm). In contrast, the BPNN model (Fig. 7b) exhibits a tighter alignment of predicted values with the diagonal reference line, indicating superior prediction accuracy and enhanced robustness, as reflected by an R^2 of 0.961 and a lower RMSE of 0.128 mm. Overall, these results confirm that the BPNN model provides a more reliable prediction of cladding depth than the SVR model.

IV. CONCLUSIONS

This study systematically examined the effects of key DLMD parameters, including laser power, scanning speed, and powder feed rate, on the geometrical characteristics of Inconel 718 clads deposited on SS 316L substrates. The results confirm that increased energy input achieved through higher laser power or reduced scanning speed leads to notable enlargement in clad width, height, and penetration depth, highlighting the sensitivity of clad morphology to processing conditions. Furthermore, the implementation of a ML-assisted NSGA-II optimization framework demonstrates strong capability in predicting and optimizing process outcomes. The developed BPNN model achieved high predictive performance (R2 = 0.965 for width, 0.952 for height, and 0.961 for depth), indicating its effectiveness in capturing complex nonlinear relationships. Overall, the findings contribute to a deeper understanding of process–structure interactions in DLMD and underscore the potential of integrating experimental and data driven approaches for process optimization in additive manufacturing.

REFERENCES

[1] M. Moradi, Z. Pourmand, A. Hasani, M. Karami Moghadam, A.H. Sakhaei, M. Shafiee, J. Lawrence, Direct laser metal deposition (DLMD) additive manufacturing (AM) of Inconel 718 superalloy: Elemental, microstructural and physical properties evaluation, Optik (Stuttg). 259 (2022). https://doi.org/10.1016/j.ijleo.2022.169018.

[2] R. Ghanavati, H. Naffakh-Moosavy, M. Moradi, Additive manufacturing of thin-walled SS316L-IN718 functionally graded materials by direct laser metal deposition, J. Mater. Res. Technol. 15 (2021) 2673–2685. https://doi.org/10.1016/j.jmrt.2021.09.061.

[3] P. Ghosal, M.C. Majumder, Anangamohan, n C. Dhyay, Study on direct laser metal deposition, Mater. Today Proc. (2018) 1250 09–12518. https://doi.org/10.1016/j.matpr.2018.02.232.

[4] J. Jamaludin, M.A. Suhaimi, S. Sharif, A.H. Ahmad, Optimizing Process Parameters in Direct Laser Metal Deposition of Ti-6Al-4V for Single-Layer Track Formation: Influence on Deposition Geometry, J. Kejuruter. 37 (2025) 3023–3033. https://doi.org/10.17576/jkukm-2025-37(6)-36.

[5] M. Mazzarisi, V. Errico, A. Angelastro, S.L. Campanelli, Influence of standoff distance and laser defocusing distance on direct laser metal deposition of a nickel-based superalloy, Int. J. Adv. Manuf. Technol. 120 (2022) 2407–2428. https://doi.org/10.1007/s00170-022-08945-3.

[6] H. Liu, X. Qin, S. Huang, L. Jin, Y. Wang, K. Lei, Geometry Characteristics Prediction of Single Track Cladding Deposited by High Power Diode Laser Based on Genetic Algorithm and Neural Network, Int. J. Precis. Eng. Manuf. 19 (2018) 1061–1070. https://doi.org/10.1007/s12541-018-0126-8.

[7] J.S. Keist, T.A. Palmer, Role of geometry on properties of additively manufactured Ti-6Al-4V structures fabricated using laser based directed energy deposition, Mater. Des. 106 (2016) 482–494. https://doi.org/10.1016/j.matdes.2016.05.045.

[8] Y. Zhang, C. Lin, Y. Tian, J. Gao, B. Song, H. Zhang, Machine learning enhanced metal 3D printing : high throughput optimization and material transfer extensibility, (2025).

[9] I. Zarin, M.A. Farahani, T. Wuest, Z. Liu, Machine Learning in Directed Energy Deposition (DED) Additive Manufacturing : A State-of-the-art Review, Manuf. Lett. 35 (2023) 689–700. https://doi.org/10.1016/j.mfglet.2023.08.079.

[10] J. Qin, F. Hu, Y. Liu, P. Witherell, C.C.L. Wang, D.W. Rosen, T.W. Simpson, Y. Lu, Q. Tang, Research and application of machine learning for additive manufacturing, Addit. Manuf. 52 (2022). https://doi.org/10.1016/j.addma.2022.102691.

[11] J.S. Lim, W.J. Oh, C.M. Lee, D.H. Kim, Selection of effective manufacturing conditions for directed energy deposition process using machine learning methods, Sci. Rep. (2021) 1–13. https://doi.org/10.1038/s41598-021-03622-z.

[12] R. Li, H. Ma, K. Zeng, H. Suo, C. Li, Y. Fu, M. Zhang, M. Zhang, X. Fang, Differential Evolution-Optimized Multi-Output Support Vector Regression-Based Prediction of Weld Bead Morphology in Wire-Fed Laser-Arc Directed Energy Deposition of 2319 Aluminum Alloy, Addit. Manuf. Front. 4 (2025) 200203. https://doi.org/10.1016/j.amf.2025.200203.

[13] P.K. Shrivastava, A.K. Pandey, Optimization of Machining Parameter during the Laser Cutting of Inconel-718 Sheet Using Regression Analysis based Particle Swarm Optimization Method, Mater. Today Proc. 5 (2018) 24167–24176. https://doi.org/10.1016/j.matpr.2018.10.211.
[14] Y. Wang, C. Zhang, J.U.N. Lu, L. Bai, Z. Zhao, J. Han, Weld Reinforcement Analysis Based on Long-Term Prediction of Molten Pool Image in Additive Manufacturing, IEEE Access 8 (2020) 69908–69918. https://doi.org/10.1109/ACCESS.2020.2986130.
[15] J. Wang, B. Zhao, Y. Liu, J. Zhao, Research Progress in Shape-Control Methods for Wire-Arc-Directed Energy Deposition, 2024.